Biomaterials Science

ROYAL SOCIETY OF CHEMISTRY

PAPER

View Article Online
View Journal | View Issue

Cite this: *Biomater. Sci.*, 2026, **14**, 871

Non-invasive transdermal delivery of peptide inhibitors of the IL-23/IL-17 axis by novel ionic liquid biomaterials for psoriasis treatment

Xiaolei Ma,†[a] Zun Wang,†[b] Mihribangvl Alip,[a] Qi Mao,[c] Cheng Zhao,[a] Huayong Zhang,[a] Genhong Yao,*[a] Lingyun Sun[a] and Lei Jiang *[b]

Psoriasis has been successfully treated by directly blocking the interleukin (IL)-23/IL-17 pathway and several inhibitors that specifically target the IL-23/IL-17 signaling axis have been approved by the Food and Drug Administration for clinical use and show excellent efficacy. However, all the approved IL-23/IL-17 axis targeting agents cannot be non-invasively delivered as topical treatment due to their biological and physicochemical properties, *e.g.*, susceptibility to degradation, large molecular size, hydrophobicity and charge. Herein, we used novel ionic liquid biomaterials, amino acid esters and octanoic acids, as a non-invasive transdermal drug delivery system for bicyclic peptide inhibitors targeted to IL-23R and IL-17A. Using phenotypical images, psoriasis area and severity index, hematoxylin–eosin, and immunohistochemistry, we demonstrate that a biocompatible ionic liquid-based topical delivery approach of peptide inhibitors alleviates psoriasis in an imiquimod-induced psoriasis mouse model. Flow cytometry of innate lymphoid cells (ILCs) within the spleen, peripheral blood, and lesional epidermis shows that treatment with ionic liquids-peptides selectively blocks and reconfigures the spectrum of skin-resident and circulating ILCs. These results provide a framework for a topical delivery approach for peptides. Our findings highlight the potential of topical administration of peptide inhibitors of the IL-23/IL-17 pathway by biocompatible ionic liquids to treat psoriasis. The main immunopathogenic mechanism of peptide inhibitors mitigating psoriasis is reconfiguration of a spectrum of skin-resident and circulating ILCs.

Received 1st August 2025,
Accepted 18th November 2025

DOI: 10.1039/d5bm01168j

rsc.li/biomaterials-science

Introduction

Psoriasis is a chronic, inflammatory skin disorder whose global prevalence is rapidly increasing,[1,2] affecting approximately 2–3% of the population, the most common type of which is plaque psoriasis, accounting for over 80% of all psoriasis cases.[3,4] In the United States, the estimated annual economic burden is as high as $112 billion.[5] The interleukin-23 (IL-23)/interleukin-17 (IL-17) axis plays a central role in the immunopathogenesis of psoriasis and related comorbidities by stimulating keratinocyte hyperproliferation and feed-forwarding circuits of perpetual T cell-mediated inflammation.[6,7] The pro-inflammatory myeloid dendritic cells release IL-23 and interleukin-12 (IL-12) that activate IL-17-secreting T cells, T helper 1 (Th1) cells and T helper 17/22 (Th17/22) cells, to produce abundant psoriatic cytokines such as tumor necrosis factor alpha (TNF-α), IL-17 and interleukin-22 (IL-22).[8] Emerging evidences from clinical trials have shown that biologics specifically targeting IL-23, IL-23 receptor (IL-23R), and IL-17A/IL-17F are effective in the substantial reduction or even elimination of psoriatic skin injury and improve the quality of life of most patients with psoriasis.[9] In addition, based on studies of skin-resident innate lymphoid cells (ILCs) for the development of psoriatic lesions, an early and intensive IL-23/IL-17 axis blockade that suppresses the convergence of IL-17-producing and IL-22-producing ILC3s could prevent the local reappearance of inflammatory plaques and prevent relapse of psoriasis.[10,11] However, all biologic agents are currently administered by either intravenous or subcutaneous injection, which restricts targeting biologics in first-line therapeutics in patients with moderate or severe psoriasis, or psoriatic arthritis.[12]

While the majority of studies have focused on intravenous or subcutaneous pathways, transdermal delivery presents new opportunities for delivering biologics that specifically target

[a]*Department of Rheumatology and Immunology, The Affiliated Drum Tower Hospital of Nanjing University Medical School, 22 Hankou Road, Nanjing 210093, China. E-mail: yaogenhong@nju.edu.cn*
[b]*NMPA Key Laboratory for Research and Evaluation of Pharmaceutical Preparations and Excipients and Department of Pharmaceutics, School of Pharmacy, China Pharmaceutical University, 24 Tong Jia Xiang, Nanjing 210009, China. E-mail: lei.jiang@cpu.edu.cn*
[c]*Abhasvara Therapeutics, Nanjing, China*
†These authors contributed equally to this work.

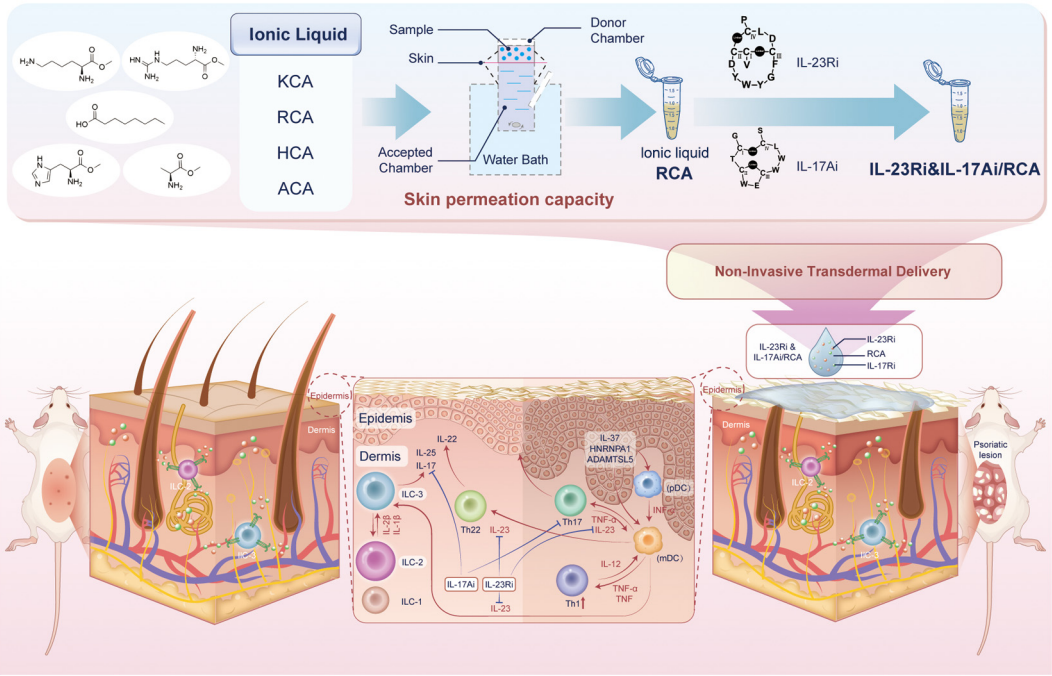

Fig. 1 Schematic illustration of non-invasive transdermal delivery of peptide inhibitors of the IL-23/IL-17 axis by biocompatible ionic liquids for psoriasis treatment.

inflammatory cytokines.[13] Topical delivery is a non-invasive transdermal approach that can enable local administration, reduce systemic exposure, and improve safety. Additionally, delivering drugs through the skin offers several advantages, such as ease of application and termination, and avoidance of first-pass metabolism, especially for patients with localized plaque psoriasis. However, topical drug delivery faces the significant challenge of the skin barrier, which under normal conditions only allows the permeation of small (<500 Da) lipophilic molecules.[14] Compared to various device-based physical methods, several formulation-based approaches, primarily involving chemical permeation enhancers, have been developed. Ionic liquids have been introduced as a novel formulation-based approach to enhance topical drug delivery for a wide range of molecules up to 150 kDa.[15] The unique advantages of ionic liquids, including chemical tunability, stability, and biocompatibility, have led to their wide application in biomedical engineering.[16] Amongst the latest investigational skin permeation approaches, ionic liquids are gaining increasing attention.[17] Ionic liquids are typically defined as organic salts composed of an organic cation and an organic or inorganic anion, which remain stable below their melting point.[18] In recent years, research on ionic liquids for protein delivery, particularly insulin delivery, has made important advances.[19] Despite decades of effort, the transdermal delivery of biological drugs remains a major pharmaceutical challenge.

Cyclic peptides have emerged as an interesting therapeutic option because they can bind to challenging targets that traditional small-molecule compounds cannot easily access. In recent studies, to develop double-bridged peptides constrained by two chemical linkers, Kong *et al.* isolated IL-17A and IL-23R target-specific peptides with nanomolar affinities that resisted proteases in undiluted simulated intestinal fluid.[20] The development of these stable and smaller bicyclic peptides with a molecular weight approaching 1 kDa is significant for the development of drugs suitable for topical or oral administration.[21] Peptide-based drugs, being smaller than proteins and antibodies, are more suitable for transdermal delivery, but converting existing bioactive peptides into topical drugs is extremely difficult.[22] For most peptides, achieving the high bioavailability and *in vivo* stability required for therapeutic applications remains challenging, prompting in-depth research into efficient peptide delivery strategies specifically for topical administration routes. Here, we used biocompatible ionic liquids, amino acid esters, and octanoic acids as a topical drug delivery approach for bicyclic peptide inhibitors targeting IL-23R and IL-17A. Specifically, we identified a combination of ionic liquids that simultaneously stabilizes peptides and enhances their penetration into the skin following topical application. In an imiquimod (IMQ)-induced psoriasis mouse model,[23] we demonstrated the efficacy of the formulation in blocking the IL-23/IL-17 axis and elucidated the possible mechanism of reconfiguration of a spectrum of skin-resident and circulating ILCs *in vivo* (Fig. 1).

Results and discussion

Synthesis and characterization of ionic liquids

The selection of ionic liquids for topical formulations is crucial to construct a biocompatible vehicle to ensure

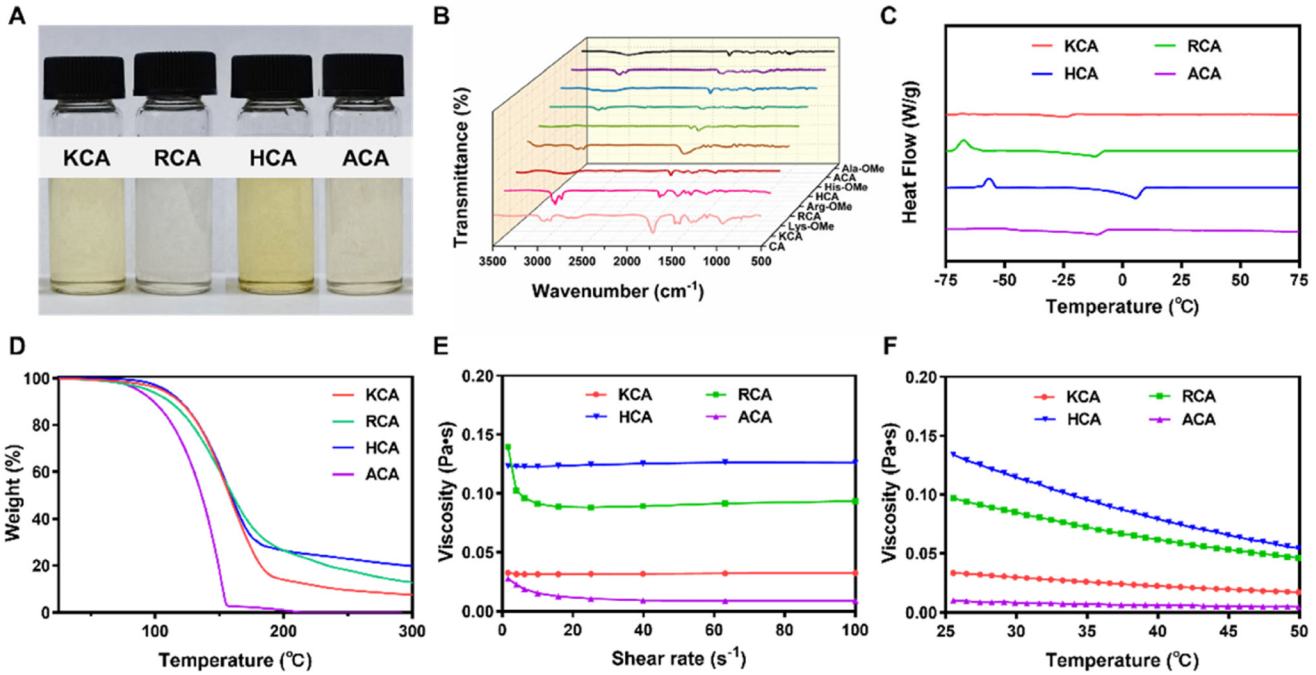

Fig. 2 Characterization of ionic liquids. (A) The appearance of the four prepared ionic liquids. (B) FTIR spectra of ionic liquids. (C) DSC thermograms of ionic liquids. (D) TGA thermograms of ionic liquids. The viscosity of ionic liquids with (E) shear rate and (F) temperature change.

maximum drug solubility together with enhanced drug permeation capacity.[18] Four amino acid ester ionic liquids, namely [Lys][C8] (KCA), [Arg][C8] (RCA), [His][C8] (HCA) and [Ala][C8] (ACA), were successfully synthesized, and their appearance was light yellow to orange-yellow, with a viscous oily form (Fig. 2A). The structures of the synthesized ionic liquids were investigated by Fourier transform infrared (FTIR) spectroscopy. The C═O vibration peak of the –COOR group in the amino acid ester structure was found at 1740–1750 cm^{-1}, and the symmetric and asymmetric C–H stretching vibrations of the methyl and methylene groups showed strong broad peaks at 2800–3000 cm^{-1}, and the same characteristic peaks are also shown for ionic liquids (Fig. 2B). The C═O stretching peak of the –COOH groups was observed at 1712 cm^{-1} in the octanoic acid spectrum, and this characteristic peak has obvious signal attenuation and blue shift in the spectra of ionic liquids. It shifted to 1706 cm^{-1} in the KCA spectrum, 1676 cm^{-1} in the RCA spectrum, 1710 cm^{-1} in the HCA spectrum, and 1709 cm^{-1} in the ACA spectrum. The shift of the characteristic peaks indicated that the product formed a carboxylate salt, and ionic liquids were successfully prepared.

The differential scanning calorimetry (DSC) results afforded the melting point temperature (T_m) and glass transition temperature (T_g) of the ionic liquids (Fig. 2C). The T_m of KCA, RCA, HCA, and ACA were −23 °C, −10 °C, 6.61 °C, and −9 °C, respectively. The higher melting point of HCA may be due to the strong intermolecular hydrogen bonds formed in ionic liquids, which need to be partially broken when melting, resulting in a higher melting point. The heat flow curves showed that T_g of RCA and HCA were −67.3 °C and −56.5 °C, demonstrating crystallization at lower temperatures. However, KCA and ACA did not exhibit this characteristic.

As seen from the thermogravimetric analysis (TGA) results (Fig. 2D), the thermal decomposition of the four ionic liquids occurred from 120 to 300 °C. The weight loss commenced at temperatures exceeding 100 °C, and the samples began displaying a substantial amount of decomposition when heated above 120 °C. KCA, RCA, and HCA still exhibited incomplete degradation products at temperatures up to 300 °C, and ACA was entirely degraded at approximately 150 °C, likely due to the stronger chemical bonds of alkaline amino acids that enhance the thermal stability of ionic liquids. The viscosity of the ionic liquids was also determined. At low shear rate conditions, as the shear rate increased, the viscosity of the ionic liquids decreased, exhibiting a shear-thinning behavior. However, when the shear rate reached 30 rad s^{-1}, the viscosity stabilized (Fig. 2E). As shown in Fig. 2F, the viscosity of the ionic liquids decreased with an increase of temperature. The high viscosity and low fluidity of HCA may be attributed to its strong intermolecular hydrogen bonding, leading to an increase in intermolecular forces. In summary, maintaining an appropriate viscosity of ionic liquids is crucial for their effective application in drug delivery on the skin surface.

Skin permeation study of ionic liquids

Transdermal administration of drugs with permeation enhancers depends on sequential penetration through the stratum corneum (SC), viable epidermis, and portions of the dermis.[24] The SC presents the most significant obstacle to transportation, with diffusivity reduced by up to 1000-fold compared to

the epidermis.[25] The SC barrier property is determined by its structure, with hydrophobic lipid matrix and keratin being the main factors of the barrier.[26] ATR-FTIR studies were carried out to evaluate the changes of lipid in the SC after incubation with ionic liquids. ATR-FTIR spectroscopy was used to gain insights into the effect of ionic liquids on the SC. As shown in Fig. 3A, the characteristic absorption peaks at ≈1650 cm^{-1} (amide I) and ≈1550 cm^{-1} (amide II) due to NH-C═O vibrations correspond to the secondary structure of keratin. The two prominent bands at 2800–3000 cm^{-1} are attributed to phospholipids and fatty acids and result from the symmetric and asymmetric stretching vibrations of CH_3 and CH_2 groups from alkyl chains. The characteristic peaks for both keratin and lipid of the SC are shown in Fig. 3A. In the amide I region, we deconvoluted a single broad peak into peaks corresponding to α helix, β sheet and β turn. Upon application of ionic liquids, the SC keratin shows significant responses, which increase the fraction of α helix structures (≈1650 cm^{-1}). A loss of α helices is a sign of protein destabilization and denaturing, while ionic liquid shows stabilizing effects on protein secondary structure. In the high wavenumber region (2800–3000 cm^{-1}), ionic liquid results in the reduction of the symmetric CH_2 stretching (≈2850 cm^{-1}) peak area. The trend of decreasing peak areas represents influences on SC lipids: lipid is extracted by ionic liquids, the lipid content is reduced and the ordered structure of the SC is destroyed.

An *in vitro* skin permeation study was performed using a Franz diffusion cell system to evaluate the effectiveness of the synthesized ionic liquids as skin-penetration enhancers for delivering model drug coumarin 6 (Cou6). The results showed that the cumulative permeabilities of Cou6/KCA, Cou6/RCA, Cou6/HCA, Cou6/ACA, and Cou6/PBS were 14.14%, 21.30%, 7.61%, 7.83%, and 2.62%, respectively (Fig. 3B). The permeation rate of the experimental group was significantly higher than that of the control group. Especially, the RCA group had the strongest skin penetration effect.

In addition, we further validated the transdermal delivery capability of the RCA system for cyclic peptide drugs (Fig. S1).

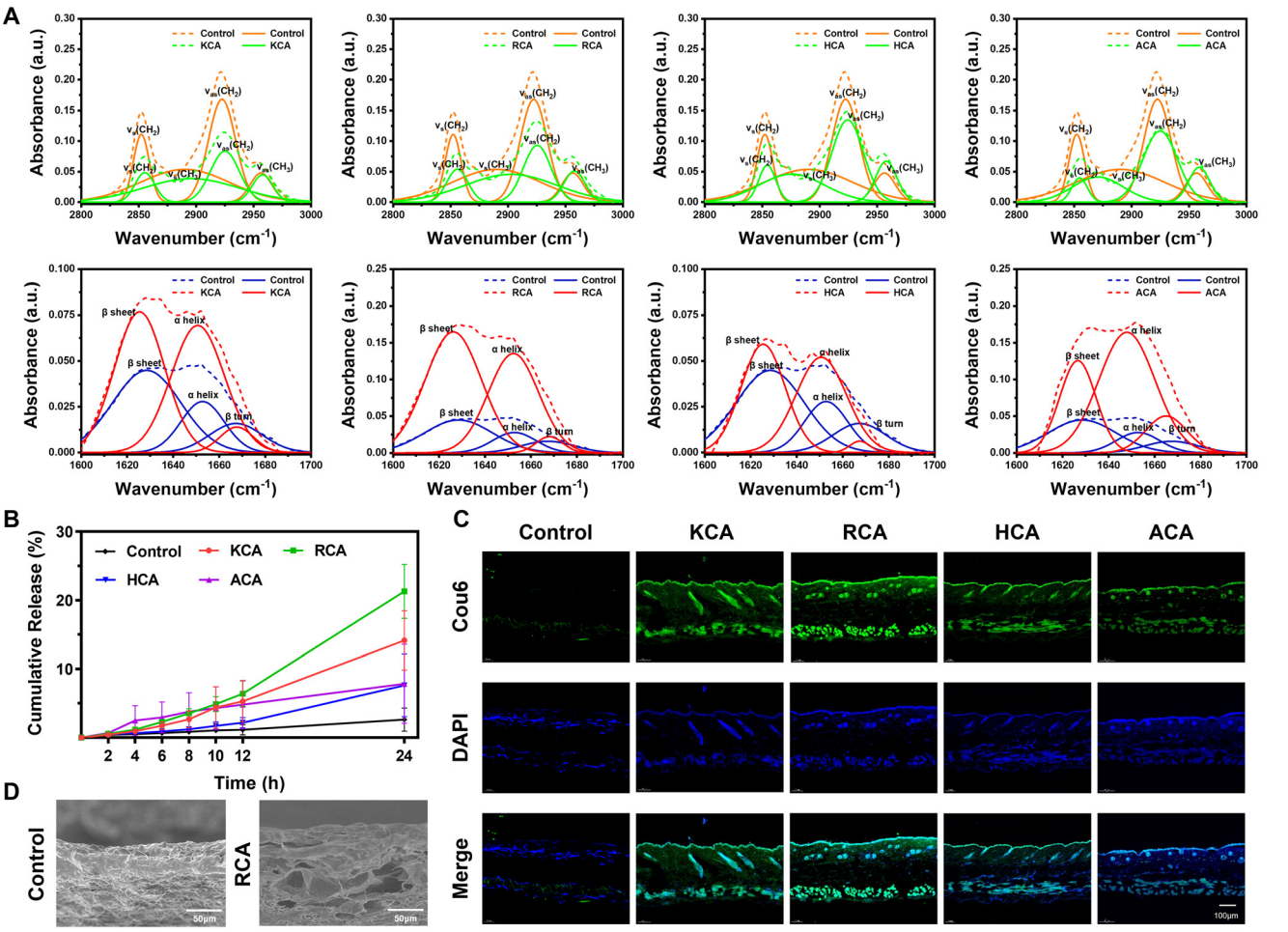

Fig. 3 Skin permeation study of ionic liquids. (A) FTIR spectra for SC samples treated with ionic liquids. Deconvoluted peaks are shown for high wavenumber region (lipid, 2800–3000 cm^{-1}) and amide I region (keratin, 1600–1700 cm^{-1}). (B) Cumulative release of Cou6 permeated across the skin over time (mean ± SD, n = 3). (C) Fluorescent images of tissue slices containing the epidermis and dermis (scale bars: 100 μm). (D) SEM image of SC cross-section after being incubated with RCA. Normal skin incubated with PBS was used as control (scale bar = 100 μm).

The 24-hour cumulative permeation rate of FITC-IL-23Ri delivered by RCA was 13.12%, representing a 5-fold increase compared to the control group (Fig. S1A). For FITC-IL-17Ai delivered by RCA, the 24-hour cumulative permeation rate was 11.12%, corresponding to a 7-fold enhancement relative to the control group (Fig. S1B). These results demonstrate that RCA is also capable of efficiently delivering macromolecular hydrophobic cyclic peptide drugs across the skin, overcoming the inherent challenge of poor skin permeation for cyclic peptide drugs attributed to their high hydrophobicity and large molecular weight. This characteristic facilitates the entry of cyclic peptide drugs into the body, enabling the operation of their pharmacological activities.

Furthermore, cyclic peptide-loaded RCA exhibits no detectable chemical structural alterations. The cyclic peptides can form hydrogen bonds with the C=O moiety of the stearic acid carboxyl groups in RCA; this interaction not only enhances drug solubility, stability, and loading efficiency but also prevents drug precipitation. As illustrated in Fig. S2, this synergistic effect ensures efficient transdermal delivery of cyclic peptides by RCA, thereby facilitating the drugs in exerting their therapeutic efficacy.

Encouraged by the impressive penetration ability of ionic liquids *in vitro*, we proceeded to assess the drug delivery efficacy *in vivo*. Following the application of different ionic liquids on skin on the back of a mouse, the remaining samples were removed, and the skin tissue was obtained for cryotomy. As shown in Fig. 3C, S3, and S4, all experimental groups showed strong green fluorescent signals of the skin tissue, indicating that the ionic liquids can effectively promote drug penetration. Semi-quantitative results showed that fluorescence could be detected in the epidermis or dermis of the experimental groups, indicating that the ionic liquids could effectively deliver drugs across the SC to the dermis. The RCA group accumulated more fluorescence in the skin, which was consistent with the results of cumulative permeation *in vitro*, and together proved that RCA had a better effect of promoting the permeation of the drug. Follow-up experiments are hence considered, using RCA as a penetration enhancer to deliver therapeutic drugs for the treatment of psoriasis.

Scanning electron microscopy (SEM) imaging exhibited the microstructural changes in the SC cross-section after ionic liquid treatment (Fig. 3D). The skin cross-section in the control group exhibited a smooth and flat surface with a distinct oily sheen, and the multilayered lipids in the SC were densely organized. In contrast, the RCA-treated SC was loose and dry, with obvious gaps between the multilayers of lipids. The SEM results were consistent with the ATR-FTIR results, which demonstrated that the ionic liquids extracted the SC, adjusted the permeability of the skin, and increased the penetration.

The barrier function of transdermal drug delivery mostly depends on the organization of the lipid matrixes and the keratin protein structure in the SC layer.[23] The ATR-FTIR spectra suggested that the ionic liquids fused with the lipids in the SC to destroy the ordered structure of the SC, and the lipid content of the SC was reduced, which led to the decrease in the spectral peak area of the lipids. In contrast, keratins treated with ionic liquids showed an increase in the area of absorption peaks within the amide I region, indicating that the ionic liquids do not have a destructive effect on the secondary structure of keratins, and, on the contrary, they may have a stabilizing effect. The SEM results were also consistent with the ATR-FTIR results, which demonstrated that the ionic liquids extracted the SC, adjusted the permeability of the skin, and increased the penetration. Furthermore, both cumulative permeability and permeation rate were significantly higher with the RCA-based formulation compared with others. Therefore, animal experiments were considered, using RCA as a delivery vehicle to load therapeutic drugs for the treatment of psoriasis.

Remission of psoriasis by the transdermal formulation of IL-23/IL-17 axis blockade *in vivo*

Treatment options of psoriasis are primarily based on the severity of the skin lesions, assessed using the Psoriasis Area and Severity Index (PASI).[1] For patients with mild or localized plaque psoriasis (PASI $\leq$ 10 or affected body surface area $<$ 5%), first-line treatments include topical corticosteroids, calcineurin inhibitors, vitamin D analogues, keratolytics, and targeted phototherapy.[27] Among the various available treatments, topical corticosteroids remain the standard of care for managing all grades of plaque psoriasis, whether as monotherapy or as an adjunct to systemic therapy. However, long-term use of corticosteroids may lead to a range of off-target and adverse effects, including epidermal and dermal atrophy, striae, folliculitis, telangiectasia, and purpura.[28] In order to reduce long-term toxicity and comprehensively enhance therapeutic efficacy, the early use of topical application of targeted inhibitors of the IL-23/IL-17 axis would be an ideal solution.

Pathogenetically, psoriatic lesions result from prominent immune cell infiltration, hyperproliferation and disturbed differentiation of epidermal keratinocytes that are provoked by immune mediators of the IL-23/IL-17 axis.[2,29,30] Therapeutic blocking of IL-23 or IL-17 can significantly reduce or even eliminate psoriatic skin lesions, improving the quality of life for most patients.[6,29] Compared to chemically synthesized small-molecule drugs, biologics targeting the IL-23/IL-17 axis are substantially more effective and may therefore be considered as first-line therapies for patients with mild or localized plaque psoriasis.[6] Unfortunately, all biologics have to be delivered *via* intravenous infusion or subcutaneous injection dosage forms, which are associated with adverse effects such as systemic inflammatory response, opportunistic infections, infusion reactions and low patient compliance due to pain, limiting mild or localized patient use.[31–33] Due to protease degradation, polar surface, large molecular size, and weight, therapeutic biologics cannot be delivered non-invasively through topical administration.[10] Additionally, small molecules are difficult or impossible to develop for cytokine targets because of the flat or featureless binding surfaces of protein–protein interactions. Cyclic peptides are a class of molecules

that have the potential to bridge the gap between small molecules and monoclonal antibodies in non-invasive transdermal administration.[34] Their larger size allows them to interact with extended surfaces where small molecules typically cannot bind, and their ring-shaped structure limits conformational flexibility, thus reducing the entropic penalty upon target binding.[35,36]

To guarantee animal safety and the valid execution of *in vivo* experiments, we initially evaluated the *in vitro* cytotoxicity and cutaneous irritation of RCA. For the *in vitro* cytotoxicity assay, cells were co-incubated with RCA solutions at concentrations ranging from 0 to 1000 μg mL^{-1} for 24 hours. Cell viability exceeded 90% across all concentrations, with cells maintaining normal growth patterns and no overt cytotoxicity observed. Notably, at low RCA concentrations, an increase in cell count was observed, suggesting a growth-promoting effect on cells and further confirming the excellent biocompatibility of RCA (Fig. S5).

Building on the *in vitro* cytotoxicity results, subsequent *in vivo* studies confirmed that topical application of RCA to the dorsal skin of mice did not induce any alterations in the morphology or structure of dorsal skin cells. Nor did it cause any cutaneous damage to the mice throughout the treatment period (Fig. S6).

To assess the therapeutic efficacy of ionic liquids-peptides, we conducted PASI, body weight and spleen index evaluation, which coincided with the total duration of topical application. The typical skin lesions, PASI scores (Fig. S7), and body weight changes from day 0 to day 12 of the IMQ-induced psoriasis model in mice are shown in Fig. 4B, D and E, respectively. Erythema, scales and wrinkles gradually appeared on the backs of the mice during the modeling period, and were most pronounced on days 6 and 7. In the later stages of the experiment, the scales gradually fell off from the modeled areas on the backs of the mice, but the erythema and thickening of the skin were still evident. For the IL-23Ri&IL-17Ai/PBS and RCA groups, the profiles of the PASI scores were almost the same as those of the IMQ model group, indicating no anti-psoriasis efficacy. After administration of IL-23Ri/RCA, IL-17Ai/RCA, and IL-23Ri&IL-17Ai/RCA, the scores of erythema, scales and wrinkles were markedly lower compared with those of the IMQ model group (Fig. 4D). The IL-23Ri&IL-17Ai/RCA group showed the lowest degree of skin erythema, scaling and thickness, indicating excellent anti-psoriasis efficacy (Fig. 4B and D). The results of PSAI score indicate that ionic liquids-peptides outperform single ionic liquids or peptides.

There was a slight decrease in body weight of the mice after the start of modeling, which leveled off by day 8 (Fig. 4E). This may be due to the fact that the IMQ cream used for modeling caused an immune response in the mice, and the mice adapted better during the subsequent treatment phase, showing a stable body weight. IMQ induces psoriasis which, in addition to exhibiting a skin inflammatory condition, also leads to hypertrophy of the spleen tissue (Fig. 4C and G). The spleens of mice in the IMQ model group were markedly hypertrophied, with significant differences in spleen weights from those of healthy mice. The spleen size of mice was significantly reduced by IL-23Ri/RCA, IL-17Ai/RCA, and IL-23Ri&IL-17Ai/RCA treatments. The data of body weight and spleen index also suggest that peptide inhibitors of the IL-23/IL-17 axis not only reverse local psoriasis-like lesions but also ameliorate systemic inflammation. After treatment, the levels of liver biochemical indicators (alkaline phosphatase [ALP], alanine transaminase [ALT], aspartate transaminase [AST]) and kidney biochemical indicators (creatinine [CREA], urea nitrogen [UN], uric acid [UA]) were all within the normal range of mouse biochemical indicators (Fig. S8).

Hematoxylin–eosin (H&E) staining was used to analyze the histopathological changes upon psoriasis induction (Fig. 5A). The skin of mice in the model group showed obvious psoriasis symptoms, such as thickening of the SC, hyperkeratosis, hypertrophy of the SC, extension of the epidermal protuberance into the dermis, and massive infiltration of inflammatory cells. In contrast, the thickness of the SC of the skin of mice was significantly reduced and the infiltration of inflammatory cells gradually subsided after IL-23Ri/RCA, IL-17Ai/RCA, and IL-23Ri&IL-17Ai/RCA treatments, and the recovery of psoriasis symptoms in the skin of mice in the IL-23Ri&IL-17Ai/RCA group was the most obvious.

Immunohistochemistry (IHC) results showed that skins treated with IL-23Ri/RCA, IL-17Ai/RCA, and IL-23Ri&IL-17Ai/RCA showed lower IL-23R, IL-17A, TNF-α and IL-22 expression than those of non-treatment or groups with only peptide inhibitor or ionic liquid treatments, further indicating that IL-23 receptor inhibitor (IL-23Ri) and IL-17 inhibitor (IL-17Ai) were successfully delivered into the epidermis and attenuated inflammatory keratinocyte proliferation (Fig. 5B–D). Moreover, the level of psoriasis-relevant lymphocytic cytokines, such as TNF-α and IL-22, in skin lesions from the IHC results revealed that their production was significantly reduced by IL-23Ri/RCA, IL-17Ai/RCA, and IL-23Ri&IL-17Ai/RCA treatments (Fig. 5E and F).

Reconfiguration of a spectrum of skin-resident and circulating ILCs in an IMQ model

ILCs are a novel family of lymphoid effector cells that serve essential roles in the early immune response, comprising both "cytotoxic" ILCs (natural killer [NK] cells) and "helper" ILCs.[37,38] "Helper" ILCs are characterized by CD127 expression and are classified into three groups based on the cytokines they produce and the transcription factors required for their development and function: interferon-γ (IFN-γ)-producing T-bet-dependent ILC1s; IL-4-, IL-5- and IL-13-producing GATA-3-dependent ILC2s; and IL-17- and IL-22-producing RORγT-dependent ILC3s.[38] These different ILC subsets are found in various lymphoid and non-lymphoid tissues and are enriched at mucosal sites, playing important roles in maintaining barrier function and innate immune defense. Tissue-resident ILCs, including quiescent cells and ILC2s, help maintain barrier function and respond to local signals. In healthy individuals, most of the effector ILCs in the skin are ILC2s, producing cytokines IL-5 and IL-13.[39,40] Some studies have

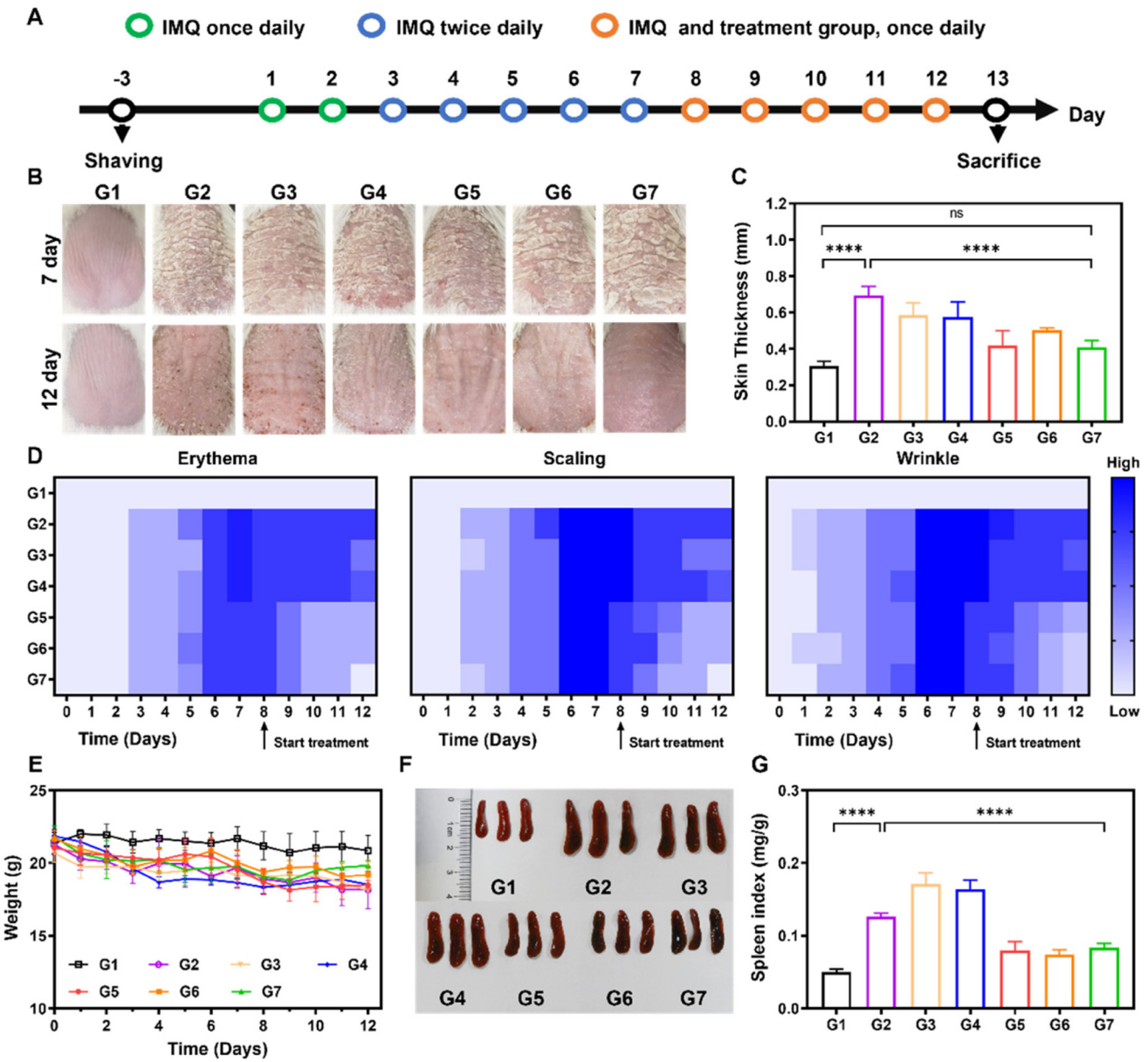

Fig. 4 *In vivo* characterization of ionic liquids-peptides in an IMQ-induced psoriasis-like mouse model. (A) Schematic illustration of psoriasis treatment. (B) Representative skin surface morphology of the various groups at day 7 and day 12. (C) Skin thickness statistics of various mouse groups. (D) PASI score (erythema, scaling, wrinkle) measured from days 0 to 12. (E) Bodyweight variations of each group from days 0 to 12. (F) Representative gross image of spleens and (G) spleen index of each group. (Mean ± SD, n = 3, ****p < 0.0001.) G1: control; G2: IMQ model; G3: IL-23Ri&IL-17Ai/PBS; G4: RCA; G5: IL-23Ri/RCA; G6: IL-17Ai/RCA; G7: IL-23Ri&IL-17Ai/RCA.

shown that inducing psoriasis in mice through IL-23 or IMQ can reconfigure a spectrum of skin ILCs, shifting them toward a pathological ILC3-like state characterized by co-production of IL-13 and IL-22 or IL-13 and IL-17A.[7,41,42]

To explore the regulatory effect of the therapeutic approach on ILC3s subtypes, we employed flow cytometry to analyze the presence and distribution of ILC3s within the spleen, peripheral blood, and epidermal tissues. Characteristic flow plots are shown in Fig. 6A and B. The quantified results indicated that, in the spleen, the total ILCs ($Lin^{-}CD127^{+}$) exhibited significant down-regulation in the model group compared to the control (Fig. 6C). Conversely, there was a discernible up-regulation of total ILCs in peripheral blood mononuclear cells (PBMCs) in the IMQ model group relative to the healthy control group (Fig. 6C). Notably, in the skin epidermis, we observed an enrichment of ILCs. Although no significant reduction was observed after treatment, a notable decreasing trend was evident (Fig. 6C). These results suggest that in the IMQ model group, there is an enrichment of ILCs in the circulatory and lesional epidermal tissues, which may originate from secondary lymphoid organs such as the spleen.

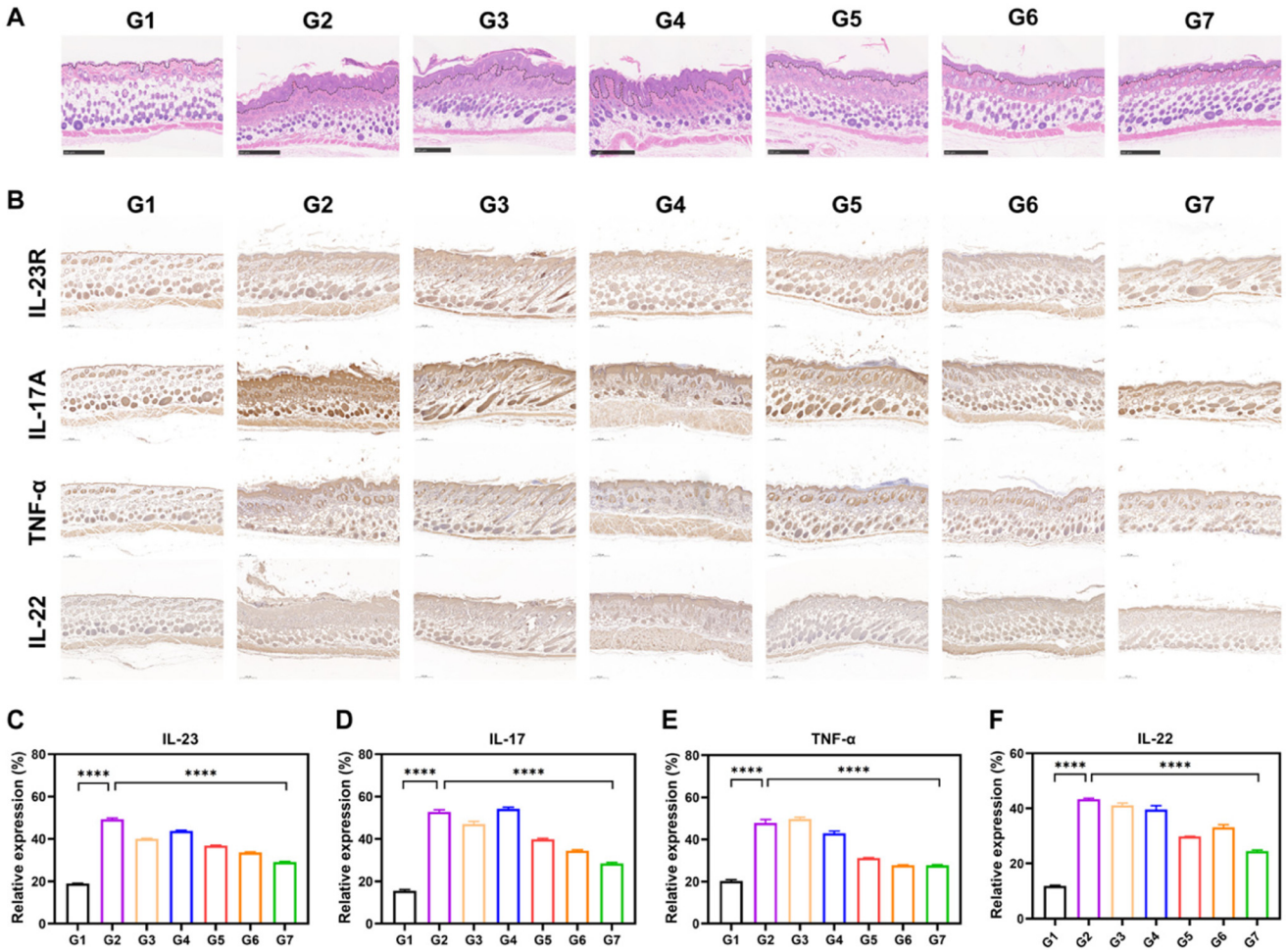

Fig. 5 Histological and immunohistochemical analysis of skin tissue sections from IMQ-induced psoriasis-like mice after treatments. (A) H&E staining images of the dorsal skin tissues in different treatment groups. Scale bar is 500 μm. (B) Representative images of IL-23R, IL-17A, TNF-α, and IL-22 expression in the dorsal skin of mice. Scale bar is 200 μm. Statistics of (C) IL-23R, (D) IL-17A, (E) TNF-α, and (F) IL-22 positive area in each group. (Mean ± SD, n = 3, ****p < 0.0001.) G1: control; G2: IMQ model; G3: IL-23Ri&IL-17Ai/PBS; G4: RCA; G5: IL-23Ri/RCA; G6: IL-17Ai/RCA; G7: IL-23Ri&IL-17Ai/RCA.

Further analysis was conducted on the RORγT$^+$ positive ILC3s. The results for ILC3s (CD127$^+$RORγT$^+$) in the spleen indicated a significant up-regulation in the model group compared to the healthy group. After treatment, groups IL-23Ri/RCA, IL-17Ai/RCA, and IL-23Ri&IL-17Ai/RCA showed a significant decrease in ILC3s (Fig. 6E). Similarly, in PBMCs and epidermal tissues, there was a significant difference between the IMQ model group and the control group, and after treatment, the IL-23Ri/RCA, IL-17Ai/RCA, and IL-23Ri&IL-17Ai/RCA groups showed a significant reduction in ILC3s (Fig. 6F and G). These results suggest that IL-23Ri/RCA, IL-17Ai/RCA, and IL-23Ri&IL-17Ai/RCA can reduce the proliferation of ILC3s, which is one of the important mechanisms by which they exert their therapeutic effects.

Here, we provide evidence that ILC3s are the major proportion of tissue-resident ILCs in psoriatic lesions, the pathogenesis of which may be dependent on the proportion switch of ILC2s to ILC3s on local exposure to IMQ. In-depth flow cytometric immunophenotypic characterization of these cells provides insights into the immunological mechanisms required for IL-23/IL-17 axis blockade peptides to restore psoriatic pathology. Notably, a significant reduction of ILC3s within the spleen, PBMCs, and skin lesions of IL-23Ri/RCA, IL-17Ai/RCA, and IL-23Ri&IL-17Ai/RCA groups reveal that peptides transdermally delivered by the ionic liquids play a crucial role in treatment of psoriasis mouse models. Further, the observation that the flow cytometric analysis of ILCs within lesional skin highly correlates with H&E and IHC results corroborates this finding. Therapeutics targeting the IL-23/IL-17 axis have been administered by intravenous or subcutaneous injections. However, we now demonstrate the efficacy of a topical formulation of ionic liquids and peptide inhibitors in IL-23/IL-17 axis selective blockade and reconfiguration of a spectrum of skin-resident and circulating ILCs and may therefore represent a potential approach for plaque psoriasis therapy.

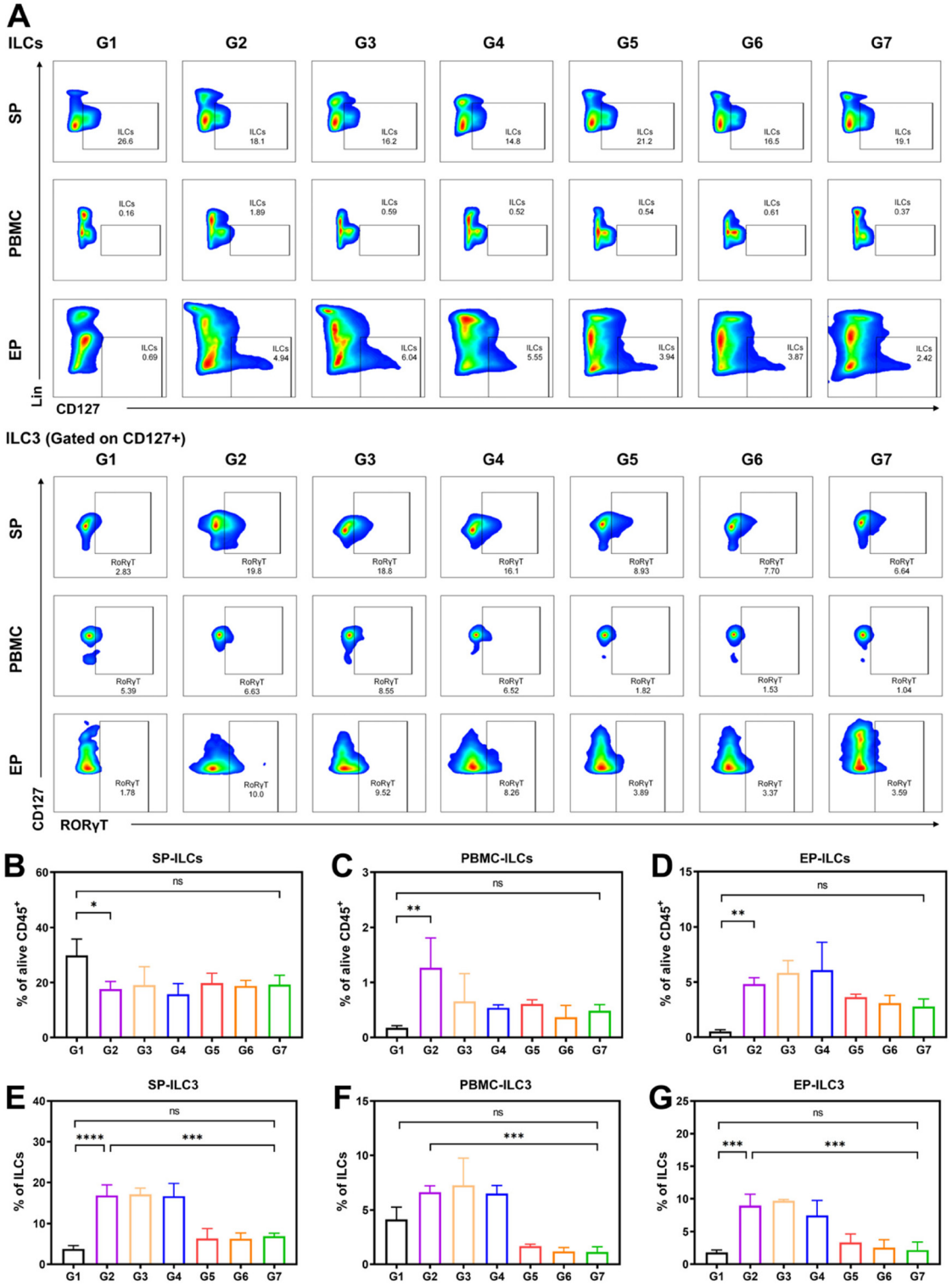

Fig. 6 Changes of splenic, peripheral blood and epidermal ILCs and ILC3 after treatment. (A) Representative flow cytometry charts of ILCs and ILC3 (RORγT$^+$) after being gated on CD127$^+$. Statistical analysis of ILCs in (B) SP, (C) PBMCs, and (D) EP. Statistical analysis of ILC3 (RORγT$^+$) in (E) SP, (F) PBMCs, and (G) EP. (Mean ± SD, n = 3, ****p < 0.0001, ***p < 0.001, **p < 0.01, *p < 0.05, ns: no significance.) G1: control; G2: IMQ model; G3: IL-23Ri&IL-17Ai/PBS; G4: RCA; G5: IL-23Ri/RCA; G6: IL-17Ai/RCA; G7: IL-23Ri&IL-17Ai/RCA.

Conclusion

Here, we present an ionic liquid formulation capable of improving the transdermal delivery of bicyclic peptides. We hypothesized that a formulation of ionic liquids would improve peptides' penetration. We validated this hypothesis in an IMQ-induced psoriasis-like skin inflammation model that resembles plaque-type psoriasis in humans. Topical application of ionic liquids-peptides for five consecutive days generated substantial reduction in PASI score, the levels of inflammatory cytokines and a spectrum of skin-resident and circulating ILCs. Our results also indicated that no skin damage and no liver or kidney toxicity were observed in the mice during the treatment period. These findings suggested that the ionic liquid-based topical delivery approach with peptide inhibitors might be a promising treatment for psoriasis patients. Our findings also indicated that these novel ionic liquid biomaterials, amino acid esters and octanoic acids, as a non-invasive transdermal drug delivery system might be used for other diseases.

Methods

Synthesis of ionic liquids

Amino acid ester hydrochloride was dissolved in methanol and slowly passed through an anion exchange resin to remove the hydrochloride. After the methanol was removed by spin evaporation, a calculated amount of octanoic acid (mole ratio of amino acid ester to octanoic acid = 1 : 4) was added to the reaction flask. The appropriate amount of methanol was added to dissolve the reactants, and the mixture was magnetically stirred at room temperature for 24 h. At the end of the reaction, methanol was removed by rotary evaporation, and an oily product was obtained adhering to the bottom of the bottle as an ionic liquid. Four amino acid ester ionic liquids, namely KCA, RCA, HCA and ACA, were successfully synthesized. The identities of the ionic liquids were investigated using FTIR spectra obtained in the range 500–3500 cm^{-1} with an accumulation of 32 scans.

Physical and chemical properties of ionic liquids

The thermal stability properties of compounds are often determined by DSC and TGA. DSC thermograms of the ionic liquids were obtained using a differential scanning calorimeter (DSC250, TA, USA). Weighed samples (<10 mg) were placed in aluminum sample trays and sealed with aluminum caps. A blank aluminum box was used as a control. The temperature increase rate was set at 2 °C min^{-1}, and the scanning temperature range was −75 °C to 75 °C. The samples were scanned three times in a cycle under a constant nitrogen flow of 30 mL min^{-1}. TGA thermograms of the ionic liquids were obtained using a thermogravimetric analyzer (TGA550, TA, USA). Samples (5–10 mg) were placed in an aluminum sample pan, and heated at 25–300 °C under a constant nitrogen gas flow at 30 mL min^{-1} (heating rate 10 °C min^{-1}) to determine the change in weight of each sample.

A rheometer (DHR-2, TA, USA) can be used to determine the viscosity of the ionic liquids, reflecting their spreadability. A parallel plate fixture was selected with a measurement temperature of 25 °C and a gap of 1 mm. The sample was loaded in the center of the sample stage, the fixture was lowered to the pre-set gap, and the sample outside the fixture was scraped off. The viscosity change was measured in the range of shear rate of 1–100 s^{-1}. The same operation was performed as above, with a fixed shear rate of 10 s^{-1}, to determine the change in viscosity of the ionic liquids over the temperature range of 25–50 °C.

Study of SC

All animal experiments followed the NIH Guide for the Care and Use of Laboratory Animals and were performed in accordance with guidelines of the Affiliated Drum Tower Hospital of Nanjing University. Mouse skin was wrapped in tinfoil and heated at 60 °C for 2 min to separate the SC. The SC was immersed in 0.25% trypsin solution overnight to digest the adherent tissues and rinsed three times with water. After drying at room temperature for 24 h, the SC was cut into 0.5 cm × 0.5 cm squares. The SC was immersed in 0.3 mL of ionic liquids and incubated for 24 h. The surface of the SC was rinsed clean of ionic liquids with water and dried at room temperature for 24 h. A control sample with PBS was also prepared under the same conditions. An ATR-FTIR spectrum of each sample was recorded in the range 500–4000 cm^{-1} with an accumulation of 32 scans. SEM imaging was used to observe the microstructure of the SC cross-section.

In vitro skin permeation study

After the mice were euthanized, the back hair was shaved off with a shaver and applied evenly with depilatory cream, which was wiped off after a few minutes. The skin on the back was peeled out with scissors and the subcutaneous fatty tissue was removed, and rinsed well with saline. The skin was wiped dry, laid flat on plastic wrap and placed in a −20 °C refrigerator prior to analysis.

For experiments, mouse skin was placed in a Franz diffusion cell (TYP-2, LTD, China) with the SC facing up. The receiving pool was added with PBS (5% Tween 80) solution until it just touched the mouse skin, excluding air bubbles. *In vitro* transdermal experiments were performed to examine the pro-osmotic efficiency of the four ionic liquids by delivering the fluorescent substance Cou6. Cou6 & PBS was used as the control group, and the experimental groups were set up as Cou6 & RCA, Cou6 & RCA, Cou6 & HCA, and Cou6 & ACA, with a concentration of Cou6 of 50 μg mL^{-1}. The receiving solution and the mouse skin were equilibrated at 37 °C for 30 min, and then 0.3 mL of the sample solution was added to the supply pool. The experiments were performed under constant magnetic stirring at a temperature of 37 ± 0.5 °C and a speed of 300 rpm. At preset time intervals (2, 4, 6, 8, 10, 12, 24 h), 1 mL of buffer solution sample was removed from the receiving pool

and an equal volume of isothermal buffer solution was immediately replenished. The sample solution was removed and the fluorescence intensity of the contained Cou6 was measured by a microplate reader (BioTek Synergy H1, Agilent Technologies, USA). After 24 h of sampling, the skin of each group was collected, rinsed and dried repeatedly, and stored at −80 °C. After performing frozen sectioning and staining, the skin was scanned to observe the accumulation of Cou6 in mouse skin.

Transdermal delivery of cyclic peptides by RCA

IL-23Ri and fluorescein isothiocyanate (FITC) were accurately weighed and separately dissolved in 2 mL of dimethyl sulfoxide (DMSO). Subsequently, the FITC solution was slowly added dropwise to the IL-23Ri solution, and magnetic stirring was maintained for a 24-hour reaction at room temperature. Upon completion of the reaction, the reaction mixture was transferred to a regenerated cellulose dialysis bag (molecular weight cutoff: 1000 Da) for dialysis. The dialyzed solution was then lyophilized to yield orange-yellow powdery FITC-labeled IL-23Ri (FITC-IL-23Ri). Using an identical protocol, FITC-labeled IL-17Ai (FITC-IL-17Ai) was prepared *via* the reaction of IL-17Ai with FITC.

FITC-IL-23Ri/PBS and FITC-IL-17Ai/PBS were designated as the control groups, while FITC-IL-23Ri/RCA and FITC-IL-17Ai/RCA were assigned as the experimental groups. The *in vitro* skin penetration assay was performed using a Franz diffusion cell system, with the temperature maintained at 37 ± 0.5 °C and a stirring rate of 300 rpm. Samples were collected from the receptor compartment at pre-determined time intervals. The fluorescence intensity of the collected samples was determined using a multifunctional microplate reader, and the concentration of the fluorescently labeled drug in each sample was calculated accordingly.

RCA stability study

IL-17Ai was precisely weighed and dissolved in RCA at a concentration of 500 μg mL^{-1}. Using RCA as the reference substance, the infrared spectral structure of IL-17Ai/RCA from 0 to 7 days was determined through FTIR spectroscopy scanning.

In vitro cytotoxicity test

NIH/3T3 cells were seeded in a 96-well plate at an appropriate density and cultured in fresh DMEM complete medium. RCA was accurately weighed to prepare serial concentrations ranging from 0 to 1000 μg mL^{-1}. Subsequently, 100 μL of the RCA solution at each concentration was added to the corresponding wells. Following 24 hours of incubation, 100 μL of MTT solution (1 mg mL^{-1}) was added to each well under dark conditions. The plate was then returned to the incubator for an additional 4-hour incubation. After incubation, the optical density (OD) of each well was measured using a microplate reader, and the relative cell viability was calculated accordingly.

Skin irritation study

After the mice were anesthetized, their dorsal hair was removed with a hair clipper, and the remaining hair was eliminated by applying depilatory cream. An ionic solution was evenly applied to the depilated skin of the mice for 5 consecutive days. On the 2nd day after the last application, the mice were anesthetized, and approximately 1 cm^2 of skin tissue was excised from the dorsal region with scissors. The skin tissue was fixed in 4% paraformaldehyde overnight, followed by paraffin embedding and sectioning into 5 μm slices. H&E staining was performed on the sections following routine protocols.

Psoriasis-like mouse models

All animal experiments followed the NIH Guide for the Care and Use of Laboratory Animals and were performed in accordance with guidelines of the Affiliated Drum Tower Hospital of Nanjing University. IMQ is a Toll-like receptor (TLR) agonist that activates natural immunity and further stimulates adaptive immunity by stimulating TLR7/8. Currently, animal models of psoriasis are often established using topical IMQ cream for induction. In this experiment, 6- to 8-week-old female Balb/c mice were selected to establish a psoriasis model by IMQ induction. The hair on the back of the mice was shaved with a shaver, and the removal area was about 2 cm × 3 cm. Depilatory cream was applied to the removal area to completely remove the hair. After depilation, the mice were put back into the cage for normal feeding and observation for 48 h. Mice with no broken or erythematous allergies on their backs were selected for subsequent experiments. Mice were daily dorsally coated with 25 mg cm^{-2} of IMQ cream to construct a psoriasis model. The amount of IMQ cream applied can be gradually increased if conditions such as no significant skin changes or reversible regression occur. The modeling period is usually 7 days, and the appearance of obvious scaly coverage, erythema, and folds on the back of the mice indicates that the mice have been successfully modeled.

In vivo evaluation of therapeutic efficacy on psoriasis mice

The mice were randomly divided into seven groups, with one group as a healthy control group (Control) and six groups induced with psoriasis by IMQ. Then, the psoriasis-bearing mice were treated with different formulations to evaluate the treatment efficiency. One group was chosen as a negative control without treatment (IMQ Model), and the other five treatment groups were administered with free bicyclic peptide inhibitors targeted to IL-23R and IL-17A (IL-23Ri&IL-17Ai/PBS), blank ionic liquid (RCA), ionic liquid delivery of IL-23R peptide inhibitor alone (IL-23Ri/RCA), ionic liquid delivery of IL-17A peptide inhibitor alone (IL-17Ai/RCA), and ionic liquid co-delivery of drug bicyclic peptide inhibitors targeted to IL-23R and IL-17A (IL-23Ri&IL-17Ai/RCA). Before administering the medication, the model area on the back of the mice was gently wiped with normal saline to remove any residual drugs from the previous administration. Mice in each group were

administered 100 μL of the corresponding preparation daily for 5 days. The corresponding drugs were applied to the model area on the back of the mice, ensuring they were evenly distributed. The administration site was gently pressed until the drugs were fully absorbed and no liquid leaked out.

PASI score was used to assess the severity of skin inflammation in a mouse model of psoriasis. The factors assessed were erythema, scaling, and wrinkling. Erythema refers to the area of erythematous rash that appears on the skin of the back of a mouse after the application of IMQ cream. Scaling refers to the degree of flaking of the skin after the appearance of symptoms of inflammation. Wrinkling refers to the degree of folding of the skin after the development of symptoms of psoriasis. Mice were assessed in descending order of severity based on their daily back conditions. The sum of the above three assessment scores was used for overall assessment of the severity of psoriasis inflammation. The scores were recorded daily from the day of the experiment, and photographs were taken to document the condition of the backs of the mice.

Body weight and spleen weight measurement

The use of IMQ cream modeling to induce an immune response in mice results in weight loss and, in severe cases, death. Body weights of mice were recorded daily to reflect the living conditions of the mice. IMQ induces an immune response in mice that produces signs of hypertrophy of the spleen tissue. At the end of the dosing treatment cycle, mice were euthanized and dissected to obtain spleen tissue, which was weighed and photographed to document spleen status.

Histopathological and immunohistochemical examination of skin

At the end of the experiment, samples of skin of mice at the dorsal modeling site were cut off and fixed with 4% paraformaldehyde. The fixed skin was dehydrated and embedded in paraffin. For histological evaluation, the paraffin blocks were sectioned into 4 μm sections and stained with H&E. A scanner (NanoZoomer 2.0-RS, Japan) was used to obtain the images of the skin sections. For IHC examination, anti-IL-23R antibody, anti-IL-17A antibody, anti-TNF-α antibody and anti-IL-22 antibody were used as the primary antibodies. The sections were incubated with diluted biotin-conjugated goat anti-rabbit IgG at 4 °C for overnight. The sections were observed under a Nikon ECLIPSE E100 microscope.

Isolation of cells from blood, spleen and skin

After euthanizing each mouse, blood, spleen, and skin tissues were harvested. For flow cytometric analysis of the skin tissues, samples were collected from the dorsal modeling area. Subsequently, each skin sample was placed face-up in 10 mL of epidermis digestion solution (containing 0.15% trypsin and 0.75 mM EDTA) and incubated for 45 min at 37 °C in a cell culture incubator. The skin samples were briefly transferred to the lids of the Petri dishes to remove the epidermis digestion solution, then placed back into the Petri dishes with the addition of 20 mL of 5% fluorescence-activated cell sorting (FACS) buffer at 4 °C. Using two curved forceps, the epidermis was gently separated from the dermis, and effective enzymatic digestion allowed for the easy detachment of the epidermal component without excessive force. Subsequently, further mechanical dissociation was carried out using a 10 mL syringe (Covidien), with 8 to 10 gentle pumps to avoid applying excessive pressure and preserving cell viability. The cell suspensions were filtered through sterile 100 mm Falcon™ Cell Strainers (Corning) positioned on 50 mL conical tubes and centrifuged at 400*g* for 5 minutes at 4 °C. After removing the supernatant, the cell pellets were resuspended in 10 mL of 5% FACS buffer. The solution was then filtered through sterile 40 mm Falcon™ Cell Strainers (Corning) placed on new 50 mL conical tubes, followed by another centrifugation at 400*g* for 5 min at 4 °C. The supernatant was removed, and the cells were resuspended in 300 mL of 5% FACS buffer. To isolate PBMCs, mouse peripheral blood was collected using a mouse peripheral blood lymphocyte separating solution. After centrifugation, the PBMCs were obtained from the buffy coat and washed with 2% FACS buffer. To obtain spleen single cell suspension, the spleen tissue was minced into small pieces and filtered using a 70-μm cell strainer. The filtered cells were washed with 2% FACS buffer. All steps should be performed under ice conditions to prove cell viability. The isolated cells can be used for downstream applications such as flow cytometry, cell sorting, or cell culture.

Flow cytometry

The obtained single-cell samples were stained using 100 mL of Zombie Aqua Fixable Viability Kit and a mixed solution of mouse IgG, then incubated at 4 °C for 15 min to assess cell viability. Following this, cell-surface antibodies were applied and incubated for 30 min at 4 °C. Subsequently, 200 μL of 13 Foxp3 fixation/permeabilization working solution was used to fix the cells, incubating them at room temperature in the dark for 30 min. Afterwards, the cells were centrifuged at 500*g* for 5 min at 4 °C, and the supernatant was discarded. The cells were then resuspended in permeabilization buffer working solution. Another centrifugation at 500*g* for 5 min at 4 °C was performed, and the supernatant was discarded. The cells were resuspended in 13 permeabilization buffer working solution containing 2% normal rat serum and incubated at room temperature in the dark for 15 min. The antibody mixture for the transcription factor RORγT was added to each sample and left at room temperature for 1 h. After subsequent washing and centrifugation steps, the cells were washed with 200 mL of permeabilization buffer working solution. They were centrifuged at 500*g* for 5 min at 4 °C, and the supernatant was discarded. Finally, the cells were resuspended in 200 mL of permeabilization buffer working solution and kept on ice until data collection. Then, cell phenotyping was performed with a flow cytometer (Agilent, USA). The cell surface antibodies used were as follows: CD127 BV421 (62-1271-82), CD45 BV711 (103147), Lin FITC (133301), RORγT PE-cy7 (25-6981-82).

Statistical analysis

Quantified data were recorded as the mean ± standard deviation (SD). Statistical analysis was performed using GraphPad Prism (GraphPad Software 8.0.2). One-way analysis of variance (ANOVA) was performed to compare two or more groups.

Author contributions

Xiaolei Ma and Zun Wang contributed equally to this work. Lei Jiang, Qi Mao and Genhong Yao developed the concepts and designed the experiments. Xiaolei Ma, Zun Wang and Mihribangvl Alip performed the experiments, measured data, and analyzed the results. Xiaolei Ma, Zun Wang, Mihribangvl Alip, Qi Mao, Cheng Zhao, Genhong Yao, and Lei Jiang analyzed the results, wrote and revised the manuscript. Lingyun Sun, Huayong Zhang, Genhong Yao, and Lei Jiang supervised the whole project.

Conflicts of interest

The authors declare no competing interests.

Data availability

All data generated or analyzed during this study are included in this published article and its supplementary information (SI). 24-hour cumulative penetration rate, FT-IR spectrum of ionic liquids RCA loaded with IL-17Ai, fluorescence intensity of Cou6 and DAPI between the epidermis and the dermis, the relative cell viability of the cells skin, H&E staining of skin, total PASI scores of psoriatic skin after the treatment and blood biochemical index are included in the SI. See DOI: https://doi.org/10.1039/d5bm01168j.

Acknowledgements

This work was supported by funding for clinical trials from the Affiliated Drum Tower Hospital, Medical School of Nanjing University (2023-LCYJ-PY-03) and the National Natural Science Foundation of China (no. 32271456). The authors acknowledge Prof. Xu-Dong Kong from Shanghai Jiao Tong University for helpful discussions.

References

1 C. E. M. Griffiths, A. W. Armstrong, J. E. Gudjonsson and J. N. W. N. Barker, *Lancet*, 2021, **397**, 1301.
2 F. O. Nestle, D. H. Kaplan and J. Barker, *N. Engl. J. Med.*, 2009, **361**, 496.
3 J. E. Greb, A. M. Goldminz, J. T. Elder, M. G. Lebwohl, D. D. Gladman, J. J. Wu, N. N. Mehta, A. Y. Finlay and A. B. Gottlieb, *Nat. Rev. Dis. Primers*, 2016, **2**, 16082.
4 A. W. Armstrong, M. D. Mehta, C. W. Schupp, G. C. Gondo, S. J. Bell and C. E. M. Griffiths, *JAMA Dermatol.*, 2021, **157**, 940.
5 E. A. Brezinski, J. S. Dhillon and A. W. Armstrong, *JAMA Dermatol.*, 2015, **151**, 651.
6 K. Ghoreschi, A. Balato, C. Enerbäck and R. Sabat, *Lancet*, 2021, **397**, 754.
7 J. E. Hawkes, B. Y. Yan, T. C. Chan and J. G. Krueger, *J. Immunol.*, 2018, **201**, 1605.
8 P. Hu, M. Wang, H. Gao, A. Zheng, J. Li, D. Mu and J. Tong, Front. Immunol., 2021, **12**, 788940.
9 K. Ghoreschi, A. Balato, C. Enerbäck and R. Sabat, *Lancet*, 2021, **397**, 754.
10 J. H. Bernink, Y. Ohne, M. B. M. Teunissen, J. Wang, J. Wu, L. Krabbendam, C. Guntermann, R. Volckmann, J. Koster, S. V. Tol, I. Ramirez, Y. Shrestha, M. A. D. Rie, H. Spits, X. R. Ros and A. A. Humbles, *Nat. Immunol.*, 2019, **20**, 992.
11 P. Bielecki, S. J. Riesenfeld, J. C. Hütter, E. T. Triglia, M. S. Kowalczyk, R. R. R. Gonzalez, M. Lian, M. C. A. Vesely, L. Kroehling, H. Xu, M. Slyper, C. Muus, L. S. Ludwig, E. Christian, L. Tao, A. J. Kedaigle, H. R. Steach, A. G. York, M. H. Skadow, P. Yaghoubi, D. Dionne, A. Jarret, H. M. McGee, C. B. M. Porter, P. L. Limón, W. Bailis, R. Jackson, N. Gagliani, G. Gasteiger, R. M. Locksley, A. Regev and R. A. Flavell, *Nature*, 2021, **592**, 128.
12 A. M. Wride, G. F. Chen, S. L. Spaulding, E. Tkachenko and J. M. Cohen, *Dermatol. Clin.*, 2024, **42**, 339.
13 A. C. Anselmo, Y. Gokarn and S. Mitragotri, *Nat. Rev. Drug Discovery*, 2019, **18**, 19.
14 Y. Ni, W. Zhao, W. Cheng, C. Deng, Z. Ying, L. Li, X. Wang, C. Sun, J. Tu and L. Jiang, *J. Controlled Release*, 2022, **351**, 245.
15 Q. M. Qi and S. Mitragotri, *J. Controlled Release*, 2019, **311**, 162.
16 Y. Xing, Y. Hu, H. Wang, Y. Diao and H. Yue, *Biomater. Sci.*, 2025, **13**, 4669.
17 A. T. Silva, C. Teixeira, E. F. Marques, C. Prudêncio, P. Gomes and R. Ferraz, *ChemMedChem*, 2021, **16**, 2604.
18 E. E. L. Tanner, A. M. Curreri, J. P. R. Balkaran, N. C. S. Wober, A. B. Yang, C. Kendig, M. P. Fluhr, N. Kim and S. Mitragotri, *Adv. Mater.*, 2019, **31**, e1901103.
19 A. Gomes, L. Aguiar, R. Ferraz, C. Teixeira and P. Gomes, *Int. J. Mol. Sci.*, 2021, **22**, 11991.
20 X. Kong, J. Moriya, V. Carle, F. Pojer, L. A. Abriata, K. Deyle and C. Heinis, *Nat. Biomed. Eng.*, 2020, **4**, 560.
21 M. Zeng, P. Deng, Q. Li, Q. Tang, J. Li and L. Zhang, *Chem. Eng. J.*, 2025, **508**, 160972.
22 C. Gorzelanny, C. Mess, S. W. Schneider, V. Huck and J. M. Brandner, *Pharmaceutics*, 2020, **12**, 684.
23 L. V. D. Fits, S. Mourits, J. S. A. Voerman, M. Kant, L. Boon, J. D. Laman, F. Cornelissen, A.-M. Mus, E. Florencia, E. P. Prens and E. Lubberts, *J. Immunol.*, 2009, **182**, 5836.
24 E. Tan, T. Wan, Q. Pan, J. Duan, S. Zhang, R. Wang, P. Gao, J. Lv, H. Wang, D. Li, Y. Ping and Y. Cheng, *Sci. Adv.*, 2024, **10**, eadl4336.

25 K. C. Madison, *J. Invest. Dermatol.*, 2003, **121**, 231.
26 C. R. Harding, *Dermatol. Ther.*, 2004, **17**, 6.
27 C. A. Elmets, N. J. Korman, E. F. Prater, E. B. Wong, R. N. Rupani, D. Kivelevitch, A. W. Armstrong, C. Connor, K. M. Cordoro, D. M. R. Davis, B. E. Elewski, J. M. Gelfand, K. B. Gordon, A. B. Gottlieb, D. H. Kaplan, A. Kavanaugh, M. Kiselica, D. Kroshinsky, M. Lebwohl, C. L. Leonardi, J. Lichten, H. W. Lim, N. N. Mehta, A. S. Paller, S. L. Parra, A. L. Pathy, M. l. Siegel, B. Stoff, B. Strober, J. J. Wu, V. Hariharan and A. Menter, *J. Am. Acad. Dermatol.*, 2021, **84**, 432.
28 A. Abraham and G. Roga, *Indian J. Dermatol.*, 2014, **59**, 456.
29 J. E. Hawkes, B. Y. Yan, T. C. Chan and J. G. Krueger, *J. Immunol.*, 2018, **201**, 1605.
30 E. Bianchi and L. Rogge, *Genes Immun.*, 2019, **20**, 415.
31 E. D. Dommasch, K. Abuabara, D. B. Shin, J. Nguyen, A. B. Troxel and J. M. Gelfand, *J. Am. Acad. Dermatol.*, 2011, **64**, 1035.
32 L. Costa, F. Caso, M. Atteno, C. Giannitti, A. Spadaro, R. Ramonda, M. Vezzù, A. D. Puente, F. Morisco, U. Fiocco, M. Galeazzi, L. Punzi and R. Scarpa, *Clin. Rheumatol.*, 2014, **33**, 273.
33 P. D. Seijo, E. Dauden, M. A. Descalzo, G. Carretero, J.-M. Carrascosa, F. Vanaclocha, F.-J. G. García, P. D. L. C. Dobao, E. H. Ceballos, I. Belinchón, J.-L. L. Estebaranz, M. Alsina, J.-L. S. Carazo, M. Ferrán, R. Torrado, C. Ferrandiz, R. Rivera, M. Llamas, R. J. Puya and I. G. Doval, *J. Invest. Dermatol.*, 2017, **137**, 313.
34 E. M. Driggers, S. P. Hale, J. Lee and N. K. Terrett, *Nat. Rev. Drug Discovery*, 2008, **7**, 608.
35 E. A. Villar, D. Beglov, S. Chennamadhavuni, J. A. Porco Jr, D. Kozakov, S. Vajda and A. Whitty, *Nat. Chem. Biol.*, 2014, **10**, 723.
36 X. Ji, A. L. Nielsen and C. Heinis, *Angew. Chem., Int. Ed.*, 2024, **63**, e202308251.
37 H. Spits, D. Artis, M. Colonna, A. Diefenbach, J. P. D. Santo, G. Eberl, S. Koyasu, R. M. Locksley, A. N. J. McKenzie, R. E. Mebius, F. Powrie and E. Vivier, *Nat. Rev. Immunol.*, 2013, **13**, 145.
38 E. Vivier, D. Artis, M. Colonna, A. Diefenbach, J. P. D. Santo, G. Eberl, S. Koyasu, R. M. Locksley, A. N. J. McKenzie, R. E. Mebius, F. Powrie and H. Spits, *Cell*, 2018, **174**, 1054.
39 B. Roediger, R. Kyle, K. H. Yip, N. Sumaria, T. V. Guy, B. S. Kim, A. J. Mitchell, S. S. Tay, R. Jain, E. F. Blom, X. Chen, P. L. Tong, H. A. Bolton, D. Artis, W. E. Paul, B. F. D. S. Groth, M. A. Grimbaldeston, G. L. Gros and W. Weninger, *Nat. Immunol.*, 2013, **14**, 564.
40 S. P. Spencer, C. Wilhelm, Q. Yang, J. A. Hall, N. Bouladoux, A. Boyd, T. B. Nutman, J. F. Urban Jr, J. Wang, T. R. Ramalingam, A. Bhandoola, T. A. Wynn and Y. Belkaid, *Science*, 2014, **343**, 432.
41 M. B. M. Teunissen, J. M. Munneke, J. H. Bernink, P. I. Spuls, P. C. M. Res, A. T. Velde, S. Cheuk, M. W. D. Brouwer, S. P. Menting, L. Eidsmo, H. Spits, M. D. Hazenberg and J. Mjösberg, *J. Invest. Dermatol.*, 2014, **134**, 2351.
42 F. Villanova, B. Flutter, I. Tosi, K. Grys, H. Sreeneebus, G. K. Perera, A. Chapman, C. H. Smith, P. D. Meglio and F. O. Nestle, *J. Invest. Dermatol.*, 2014, **134**, 984.